

# First local seismic tomography for Red River shear zone, northern Vietnam: Stepwise inversion employing crustal P and P<sub>n</sub> waves

Hsin-Hua Huang<sup>a,b,\*</sup>, Zhen J. Xu<sup>b</sup>, Yih-Min Wu<sup>a</sup>, Xiaodong Song<sup>b,\*\*</sup>,  
Bor-Shouh Huang<sup>c</sup>, Le Minh Nguyen<sup>a</sup>

<sup>a</sup> Department of Geosciences, National Taiwan University, No. 1, Roosevelt Rd. Sec. 4, Taipei 10617, Taiwan

<sup>b</sup> Department of Geology, University of Illinois, Urbana, IL 61801, USA

<sup>c</sup> Institute of Earth Science, Academia Sinica, No. 128, Sec. 2, Academia Road, Nangang, Taipei 115, Taiwan

## ARTICLE INFO

### Article history:

Received 14 November 2011  
Received in revised form 2 February 2012  
Accepted 23 March 2012  
Available online 3 April 2012

### Keywords:

Red River shear zone  
Northern Vietnam  
Local seismic tomography  
P<sub>n</sub> wave  
Moho depth

## ABSTRACT

The 900-km-long Red River shear zone (RRSZ) lends a compelling support to the continental extrusion model for the tectonic evolution of southeastern Asia, but has been challenged by many of views, as some new records mainly from northern Vietnam, suspecting the dimensions of RRSZ neither in depth nor in displacement are as large as we expected before. However, compared to the northwestern half of the RRSZ in Yunnan province better studied by many fields, the southeastern half in northern Vietnam is relatively poorly constrained by seismic study, due to insufficient stations and data in the past. This study, using a newly deployed portable broadband seismic network, obtained the first local seismic tomography with a stepwise inversion using P and P<sub>n</sub> phases. Surface geology, major structures, and rock properties are well correlated and identified in our model, suggesting the RRSZ is a lithospheric structure at least penetrating to the uppermost mantle with mantle thermal anomalies. In general, the crust of northern Vietnam appears to be weak and sits on a relatively hot uppermost mantle, showing a long and complex thermo tectonic history. A mid-lower crustal segmentation of RRSZ is also proposed to compromise the discrepancies recently observed between Yunnan province and northern Vietnam.

© 2012 Elsevier B.V. All rights reserved.

## 1. Introduction

The Red River shear zone (RRSZ) is one of the most profound geologic features in southeastern Asia, which extends over 900 km from southeastern edge of the Tibetan plateau to the Tonkin Gulf, northern Vietnam, and as far as the South China Sea. With 500–900 km in extensive left lateral displacement (Chung et al., 1997; Lan et al., 2001; Leloup et al., 1995), and the onset time of 21–27 Ma after the beginning of India–Eurasia collision ca. 50 Ma (Leloup et al., 1995; Tapponnier et al., 1990; Wang et al., 1998, 2000), the RRSZ provides prominent, original evidence for the continental extrusion model (Tapponnier et al., 1982, 1986), which attributes a significant amount of continental shortening of the India–Eurasia collision to the southeastward extrusion of the Indochina block. Therefore the RRSZ is commonly considered as a lithospheric suture separating Indochina from South China (Leloup et al., 1995; Tapponnier et al., 1990; Zhang and Schärer,

1999). However, this has been examined and challenged from many points of view. New analysis of structural fabrics within the Day Nui Con Voi (DNCV) metamorphic complex (Fig. 1), for example, suggests that the RRSZ is purely an upper crust structure that shears and exhumates the pre-existing metamorphic massif (Searle, 2006; Yeh et al., 2008). The observations from seismic profiles conducted in offshore Tonkin Gulf shows only tens of kilometers of sinistral movement against the dimension of the RRSZ displacement (Rangin et al., 1995). Moreover, according to the alignment of mafic–ultramafic belts and high potassic Paleogene magmas (Fig. 1), it is proposed that the Song Ma Fault (SMF) ought to be a better candidate of plate suture, and the RRSZ may originate by the crustal weakening of intraplate extension ca. 30–40 Ma (Chung et al., 1997; Lan et al., 2000). Central to these arguments is the spatial variation of the rheological and petrologic properties of the lithosphere along the RRSZ as well as other major structures, e.g. SMF. For instance, could the distinct properties be detected across structures, or would the Moho geometry responds to the thermal episodes, such as intraplate extension? Seismic tomography could be one of the most effective tools to image the subsurface structures to address this issue and interpret related tectonic features.

A number of tomographic studies have been done for the RRSZ in past decade with various patterns of velocity anomalies along this fault zone (Huang et al., 2002; Lei et al., 2009; Wang et al., 2003; Wu et al., 2004; Xu et al., 2005). Using P waves from local earthquakes, Huang et

\* Corresponding author at: Department of Geosciences, National Taiwan University, No. 1, Roosevelt Rd. Sec. 4, Taipei 10617, Taiwan. Tel.: +886 233664956; fax: +886 23644625.

\*\* Corresponding author. Tel.: +1 217 714 5125; fax: +1 217 244 4996.  
E-mail addresses: [d98224004@ntu.edu.tw](mailto:d98224004@ntu.edu.tw) (H.-H. Huang), [zhenxu2@illinois.edu](mailto:zhenxu2@illinois.edu) (Z.J. Xu), [drymwu@ntu.edu.tw](mailto:drymwu@ntu.edu.tw) (Y.-M. Wu), [xsong@illinois.edu](mailto:xsong@illinois.edu) (X. Song), [hwbs@earth.sinica.edu.tw](mailto:hwbs@earth.sinica.edu.tw) (B.-S. Huang), [nlminh79@yahoo.com](mailto:nlminh79@yahoo.com) (L.M. Nguyen).

<sup>1</sup> Currently visiting at University of Illinois at Urbana-Champaign.

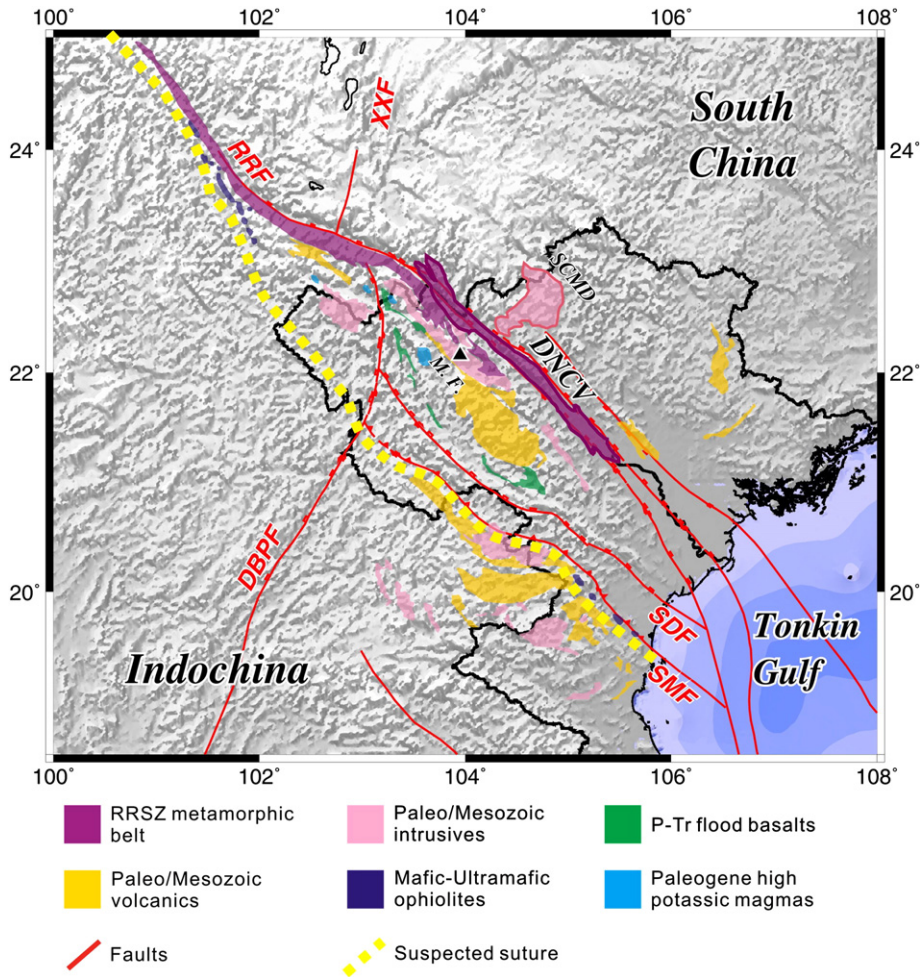


**Fig. 1.** Geologic map showing igneous rock divisions (referred to Chung et al., 1997) and geologic units. DNCV, Day Nui Con Voi metamorphic complex; SCMD, Song Chay Metamorphic Dome; M. F., Mountain Fansipan. Igneous rock types are denoted in Legend (P–Tr, Permian–Triassic), and the red line and the yellow dotted line represent the fault traces and suspected plate suture between South China and Indochina blocks. RRSZ, Red River shear zone; DBPF, Dien Bien Phu Fault; XXF, Xianshuihe–Xiaojiang Fault; SMF, Song Ma Fault; SDF: Song Da Fault.

al. (2002) obtained the tomographic images in Yunnan province, China, showing a contrast of high and low velocity anomalies across the RRSZ, which be traced down to the mantle. This feature is also confirmed by a local S wave tomography (Wang et al., 2003) and a regional surface wave tomography (Wu et al., 2004). On the contrary, in Yunnan province, the models inverted by using both local and teleseismic datasets suggest a high velocity zone in the upper crust underlined by a low velocity zone in the mid-lower crust along the RRSZ (Lei et al., 2009; Xu et al., 2005). Hindered by the lack of stations in northern Vietnam, most of these models are either the local studies focusing on the Yunnan province (Huang et al., 2002; Lei et al., 2009; Wang et al., 2003; Xu et al., 2005), or are the regional studies not capable of the detailed spatial resolution in northern Vietnam (Wu et al., 2004). Along the 900-km-long RRSZ from SE edge of Tibetan plateau to SCS, the northern Vietnam appears as a gap of the seismic investigation.

The first local seismic tomographic study of northern Vietnam became feasible, when a portable broadband seismic network was installed during the December of 2005 with the aim to image and interpret crustal and mantle structures beneath northern Vietnam (Huang et al., 2009). In this study, we combine the datasets from the Vietnam short-period seismic network (VSPSN) and the portable broadband seismic network (PBSN) (Fig. 2) in an attempt to improve the resolution of the 3D crustal and uppermost mantle structure beneath the northern Vietnam and the southeastern half of the RRSZ. We use crustal P, secondary crustal P, and  $P_n$  waves to invert for crustal and  $P_n$  velocities, as well as Moho variation.

## 2. Tectonic settings

### 2.1. Igneous rocks in northern Vietnam

The terrain of northern Vietnam consists of the South China block to the northeast and the Indochina block to the southwest, which are separated by the NW–SE suture zone of the RRSZ (Fig. 1). Along the RRSZ, a metamorphic belt is exposed over a great length from Xuelongshan, through Diancangshan and Ailaoshan in Yunnan, and extending into northern Vietnam, where the segment is called the Day Nui Con Voi (DNCV) metamorphic complex, consisting of high-grade gneiss and low-grade schist. In and around northern Vietnam, a long and complex magmatism history is revealed by various phases of igneous rocks. They can be categorized into five main groups: (1) Paleo/Mesozoic volcanics, (2) Paleo/Mesozoic intrusives, (3) P–Tr flood basalts, (4) Paleogene high potassic magmas, and (5) mafic/ultramafic ophiolites (Chung et al., 1997; Lan et al., 2000; Wang et al., 2000). The Paleo/Mesozoic volcanics and intrusives are extensively distributed, but in contrast, the P–Tr flood basalts and Paleogene high potassic magmas are located only between the RRSZ and the Song Da Fault (SDF). The mafic/ultramafic ophiolites locally fringe to the south side of the RRSZ (102.0°, 23.5°) and the SMF (105.5°, 19.5°). Of those Paleo/Mesozoic intrusives, the intrusive massif to the southwest of the RRSZ formed the highest summit of northern Vietnam called Mount Fansipan; and to the northeast of the RRSZ, the intrusive massif at Song Chay is namely the Song Chay metamorphic dome (SCMD) that is reported to have

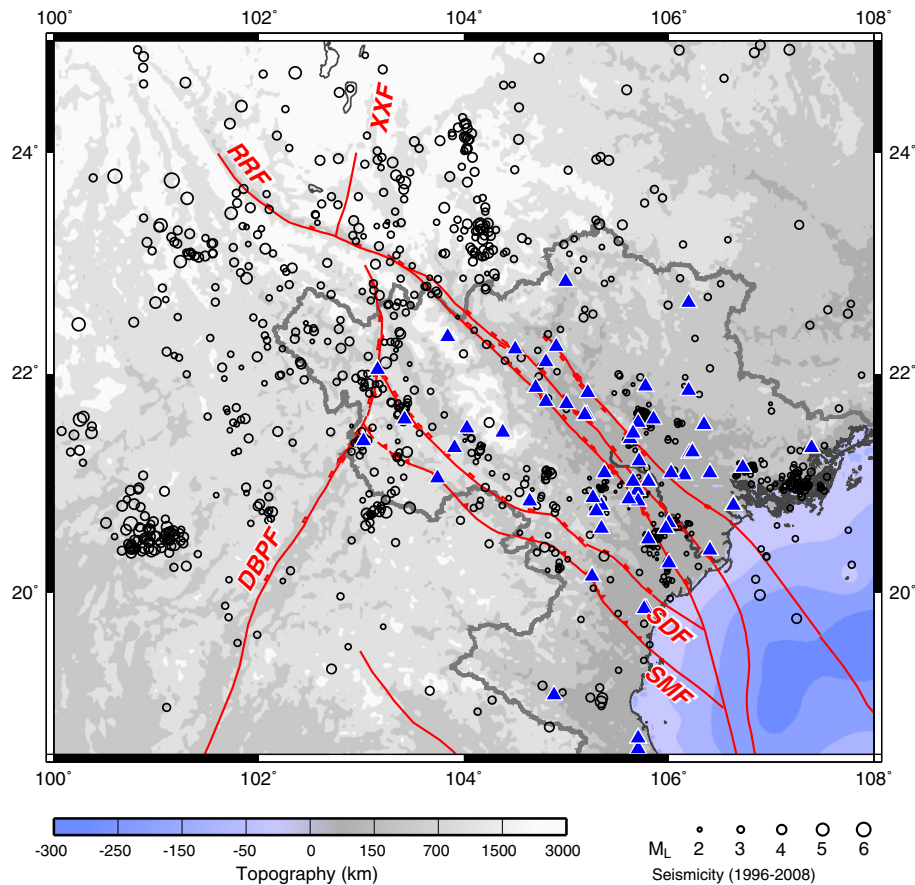


**Fig. 2.** Seismicity map of northern Vietnam. Earthquakes and stations are denoted by black circle and blue triangle, respectively. Background color shows the topography relief, and red line represents the fault trace (for abbreviations, see caption of Fig. 1).

experienced a prolonged thermal history and regarded as the evidence of the pre-existing metamorphic massif prior to the developing of the RRSZ (Searle, 2006). In addition, the outcrop of the mafic/ultramafic ophiolites, comprising fragmentarily serpentized gabbro-dolerites, harzburgites, and dunites, indicates an existence of a paleo-subduction system, and is suspected to be a better plate suture rather than the RRSZ (Fig. 1. Chung et al., 1997; Leloup et al., 1995; Trung et al., 2006).

## 2.2. Seismic activities and featured faults

Seismic activity in northern Vietnam is relatively low when compared to the surrounding regions (Fig. 2). Half of the earthquakes recorded by the seismic networks are from Yunnan province, China to the northwest, and from Laos to the west. The level of seismic activity along the RRSZ also appear to be quite low, which agrees with the current phase of the RRSZ turning into the dextral shearing, with only minor offsets within a range of tens kilometers (Allen et al., 1984; Cong and Feigl, 1999; Leloup et al., 1995; Zhu et al., 2009). The RRSZ splits into two strand faults in northern Vietnam. This wider shearing system is suggested as a flower structures which might be developed with normal components in a transtension stage of RRSZ during 15.5–30 Ma, possibly related to the spreading of SCS (Rangin et al., 1995; Searle, 2006). Within the shear zone, some narrow, NW–SE elongated depressions are then formed and distributed. On the other hand, the Dien Bien Phu Fault (DBPF) is the most active structure in northern Vietnam at present. Many earthquake clusters seem to be distributed along the DBPF and around the junction of the DBPF with the SDF and SMF. Like the RRSZ, the DBPF also has two phases of shearing from dextral in the past, to sinistral movement presently.

The RRSZ and the DBPF are therefore suspected to be a conjugate fault system under the regional deformation in southeastern Asia (Zhuchiewicz et al., 2004). The mafic/ultramafic belts mark the NW–SE striking SMF as a subduction front/suture zone for at least 170 km in northern Vietnam. To its northeast, the SDF represents a fault system of orogenic belt with tightly folded Permian mafic volcanics, Triassic shales and limestones, and Cretaceous continental red beds (Leloup et al., 1995). Although the SMF and SDF are the products of paleo-orogeny, some seismic activities are still present in this region. The Xianshuihe–Xiaojiang Fault (XXF) is another active fault with relatively high seismicity. However, it is out of our scope of this study, which focuses mainly on the tectonics of northern Vietnam.

## 3. Data and basic data processing procedure

### 3.1. Data descriptions

Our dataset contains the earthquake catalogs from the VSPSN over a time span of 1996–2008 and from the PBSN (Huang et al., 2009) over a period of 2006–2010. For the overlapping period from 2006 to 2008 between the two networks, we keep the data separate without re-associating and re-locating the phases of the same events. This is due to concerns on the errors from different operating systems, and therefore, it is worth noting that the number of earthquakes in our catalogs will be somewhat larger than the real number. Within a region of longitude 100–108°E and latitude 18.5–25°N, a total of 898 earthquakes and 51 stations are selected and used in this study (Fig. 2), comprising 6482 travel time picks of crustal P and  $P_n$  waves. The secondary P wave arrival at distances greater than the crossover distance

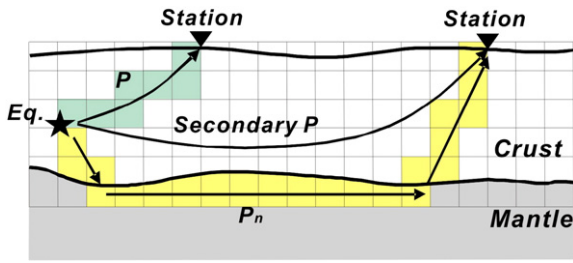


**Fig. 3.** Schematic illustration of crustal P and  $P_n$  wave phases used in this study. At small distances, P waves arrive as first arrivals sampling shallow crust. As distance increases, P wave incident upon the Moho become critically refracted at the top of the mantle and arrive at the surface as head waves, nominated  $P_n$  waves in general. At distances greater than the crossover distance,  $P_n$  waves become first arrivals and P waves arrive as secondary arrivals, sampling the mid and lower crust. Blue and yellow cells represent the discrete 3D model spaces of crust sampled by crustal P waves and 2D model spaces of mantle-lid sampled by  $P_n$  waves.

of P and  $P_n$  waves are also included as long as they are identified and picked. These secondary arrivals are abundant in our catalogs at the epicenter distance ranging from 200 to 700 km (Fig. 4a) that considerably increase the sampling rays in mid and lower crusts. Generally, most raw picks are closely clustered along the apparent travel time curves (Fig. 4a). However, some outliers and misidentifications are still present and need to be sorted out.

3.2. Stepwise procedure of this study

In this study, we explored an iterated scheme recently developed by Xu and Song (2010) to jointly invert 3D crustal P and  $P_n$  velocities and Moho maps. First, the scheme determines the 1D velocity model and re-associates the wave phases simultaneously. In the wave phase re-association, the predicted travel times of each earthquake–station pair are calculated for crustal P wave and  $P_n$  wave, respectively. The observed phase is associated with crustal P or  $P_n$ , depending on the closeness of the predicted travel times to the observed travel times. If the difference between the predicted and observed travel times is greater than 2 s, the phase is discarded (Fig. 4b).

Second, we invert the 3D crustal P and  $P_n$  velocities separately. This is a variation from the joint inversion approach for crustal P and  $P_n$  simultaneously (Xu and Song, 2010). Because of the rather uneven distribution of the P and  $P_n$  data sets, such a joint inversion, which seeks to minimize the total residuals of the least square system, can

be overly affected by the larger data set (P waves). Thus, a more straightforward way is to deal with them separately. Although some benefits of joint inversion will diminish, e.g. the contributions on crustal velocity model from  $P_n$  waves, we can more fairly assess the improvement of the inversions and the effects from the uneven data step by step.

Thus, a stepwise procedure is developed as such: (1) imposing 1D joint-inversion scheme on raw travel time picks to re-associate and filter out the picks of crustal P and  $P_n$  waves (Fig. 4), and obtain the reference 1D velocity model, including Moho depth, (2) relocating and updating earthquake hypocenters using the reference 1D velocity model and re-associated phase arrivals, (3) inverting the 3D crustal velocities using both the first and second crustal P wave arrivals, (4) with 3D crustal velocity models obtained from step (3), inverting the mantle-lid velocities using  $P_n$  wave arrivals, and (5) deriving the regional Moho variation with updated crustal P and  $P_n$  velocity models. This procedure iterates from step (2) to (4) for better refining of the earthquake locations with updated 3D velocity models and for improving velocity models with relocated hypocenters (Fig. 5). Using the final earthquake locations and both crustal P and  $P_n$  velocity models, the Moho depth variation is obtained. During each step and iteration, the travel time residuals (relative to the reference model) larger than 2 s, and earthquakes with depth deeper than the Moho are discarded.

4. Methodology

4.1. Tomographic inversion method

We follow the basic joint inversion formulation outlined in Xu and Song (2010) with some modification. The travel time residual for crustal P wave from event  $j$  to station  $k$  in a discrete form can be expressed as following:

$$r_{jk} = T_{jk}^{obs} - T_{jk}^{pred} = \sum_{c=1}^n \left( -\frac{dl}{v} \right) \left( \frac{\Delta v}{v} \right)_c, \tag{1}$$

where  $T_{jk}^{obs}$  is the observed travel time,  $T_{jk}^{pred}$  is the predicted travel time,  $n$  is the number of grids that ray path samples in the crust, and then  $dl$  and  $\frac{\Delta v}{v}$  are the length and the velocity perturbation corresponding to each grid.

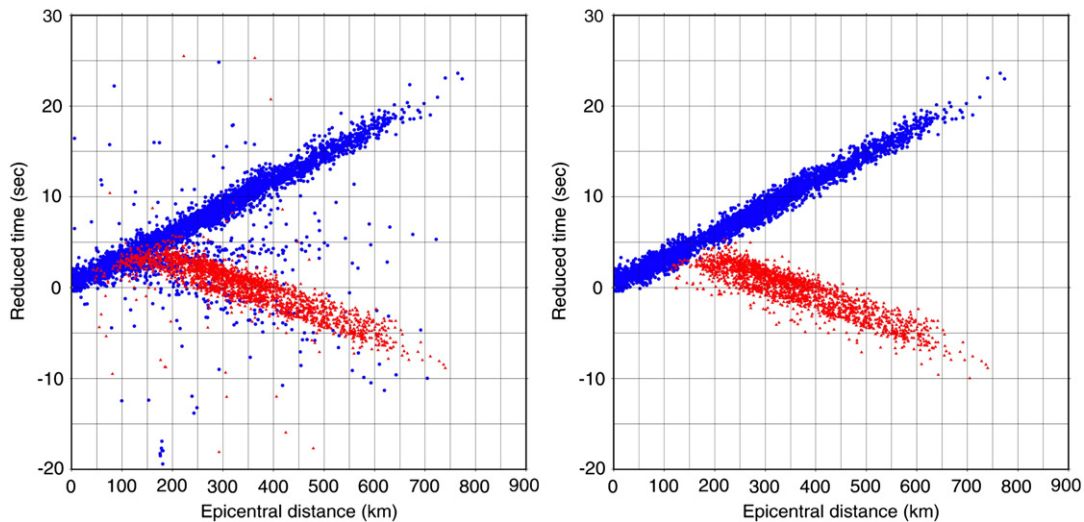


**Fig. 4.** Travel time curve reduced by 7 km/s. (a) Before and (b) after applying the 1D joint-inversion scheme (Xu and Song, 2010) on raw data. Within a 2 s misfit, in a total of 4632 crustal P and 1969  $P_n$  picks are sorted out and used in this study.

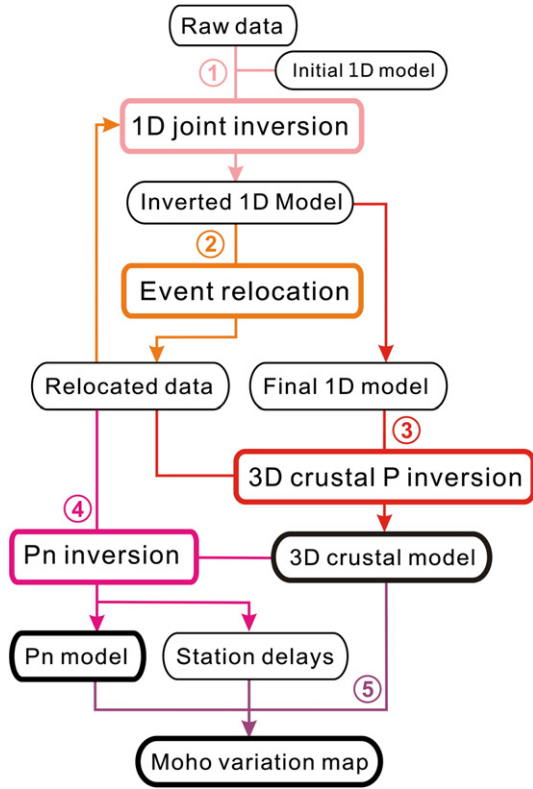


**Fig. 5.** Flow chart of the stepwise inversion procedure. Arrows show the order of steps: (1) imposing 1D joint-inversion scheme to obtain the inverted 1D velocity model (as well as the re-association of crustal P and P<sub>n</sub> phases); (2) relocating and updating earthquake hypocenters; (3) inverting 3D crustal P-wave velocities; (4) inverting mantle-lid P<sub>n</sub>-wave velocities; and (5) deriving the regional Moho variation. See text for the details (Section 3.2).

Comparably, the travel time residual for P<sub>n</sub> wave can be written as:

$$r_{jk} = T_{jk}^{obs} - T_{jk}^{pred} = \sum_{m=1}^{n_1} \left( -\frac{dl}{v} \right) \left( \frac{\Delta v}{v} \right)_m + \sum_{e=1}^{n_2} \left( -\frac{dl}{v} \right) \left( \frac{\Delta v}{v} \right)_e + \sum_{s=1}^{n_3} \left( -\frac{dl}{v} \right) \left( \frac{\Delta v}{v} \right)_s + \Delta t_j^{eq} + \Delta t_k^{st}, \quad (2)$$

where  $n_1$ ,  $n_2$ , and  $n_3$  are the number of grids that ray path samples in the mantle and at earthquake and station sides in the crust (Fig. 3). Different from the conventional formulation of P<sub>n</sub> tomography (Hearn, 1984, 1996; Liang et al., 2004), we follow the strategy of Xu and Song (2010) to actually trace the ray path of P<sub>n</sub> wave so that the portion of velocity perturbation in the formula comes to three sections as stated above. Therefore  $\Delta t_j^{eq}$  and  $\Delta t_k^{st}$  turn into the travel time delays contributed from the “Moho depth variation”, not the “Moho depth” (i.e. crustal thickness, Hearn, 1984), at the earthquake and station sides, which is written as:

$$\Delta t = \eta \Delta H, \quad (3)$$

where  $\Delta H$  is the Moho depth variation. Parameter  $\eta$  is the vertical slowness able to be calculated by the formula  $\eta = \sqrt{\left(\frac{1}{v_c}\right)^2 - \left(\frac{1}{v_m}\right)^2}$  where  $v_c$  and  $v_m$  are the velocity at the depth right above the Moho in the crust and the P<sub>n</sub> velocity in the mantle, respectively. Thereby, once we derived the crustal P and P<sub>n</sub> velocity models at steps (3) and (4), based on the following formula:

$$H = \bar{H} + \frac{\Delta t}{\eta}, \quad (4)$$

we can obtain the regional variation of the Moho depth (i.e. crustal thickness) in our study area.  $\bar{H}$  is the reference Moho depth derived from the 1D joint-inversion scheme at step (1). It is important noting that for the Eq. (2), we only invert the first, fourth and fifth terms for P<sub>n</sub> velocity perturbations, earthquake delays, and station delays. The second and third term are directly calculated by the crustal velocity model from step (3).

We apply the LSQR algorithm (Paige and Saunders, 1982a, 1982b) to solve the linearized Eqs. (1) and (2) by minimizing the least square system:  $\|Gm - d\|^2 + \lambda^2 \|m\|^2 + \varphi^2 \|Lm\|^2$ . Here  $m$  is the model vector that is the velocity perturbation we would like to obtain,  $d$  is the data vector whose entries are the residuals ( $r_{jk}$ ) between predicted and observed travel times, and  $G$  is the kernel matrix composed of partial differential coefficients that links up the vector  $m$  and  $d$ . The first term therefore represents the misfit of equations. And furthermore, because of the nature of uneven distribution of earthquakes and stations, tomographic inversion problems are generally highly ill-conditioned and cause instability during inversion. To overcome this, a common approach is to impose the regularization on ill-conditioned systems with additional constraints, such as damping and smoothing constraints. By this concept, the second term is the magnitude of model vector itself with a damping factor  $\lambda$  to suppress the overreaction of the model norm. Then the third term represents the smoothing constraint, where  $L$  is the finite difference Laplacian operator (Lees and Crosson, 1989) in charge of the roughness over the model space, and the coefficient  $\varphi$  is the factor to control the level. After a number of empirical tryouts,  $\lambda$  and  $\varphi$  are chosen as 5 and 10 for crustal P wave inversion, while for P<sub>n</sub> wave inversion they are chosen as 10 and 10 in this study.

Because the Eq. (2) contains quantities with different units, we apply a preconditioning matrix  $P$  to make the kernel matrix  $G$  dimensionless in P<sub>n</sub> tomographic inversion.  $P$  is a diagonal matrix whose diagonal elements are the reciprocal of the  $L_2$  norm of each column vector  $c$  in kernel matrix  $G$ . This process makes  $G' = GP$ ,  $m' = P^{-1}m$ , and does not change the linear system as  $G'm' = GPP^{-1}m = d$ . To the end, the real model vector can be recovered by  $m = Pm'$  reversely.

#### 4.2. Earthquake relocation method

Sometimes, tomographic inversions are carried out by involving source parameters (hypocenter location and original time) into the formulation (Zhang and Thurber, 2006). However, such a formulation generally relies on the assumption that the earthquake mislocation is small enough to achieve a linearized system with velocity disturbances simultaneously. Otherwise, the errors of mislocation will be directly mapped into the tomographic inversion, and will produce artificial anomalies that mask the real structure signals. Furthermore, the speed of convergence of earthquake parameters is generally different from that of the earth structure parameters. Hence, the earthquake relocation prior to the tomographic inversion is suggested in most situations for deriving a better starting model of event locations (Van der Hilst and Engdahl, 1992).

In the case of northern Vietnam, it is highly desirable that a prior-to-inversion relocation is done as it is evident that a large percentage of earthquakes have artificial fixed depth in the raw earthquake catalog. Here, we apply the analytical kernel matrix on crustal P and P<sub>n</sub> waves (Gubbins, 1990), and formulate a weighted, damped least square system:  $\|WGm - Wd\|^2 + \lambda^2 \|m\|^2$ , where  $W$  is the diagonal weighting matrix whose elements are normalized to a range of 0 to 1 by the residual between predicted and observed travel times. The second term is a damping constraint as described in tomographic inversion. Compared with the relocation of common fashion that only uses the first P wave arrivals, our relocation exhibits some advantages. First, to draw support from the 1D joint-inversion scheme, we can fairly re-associate the crustal P and P<sub>n</sub> wave arrivals and trace both ray paths adequately without the phase contamination. Second, the recognition of the secondary P arrivals earns us more constraints for

hypocenter determination than only using the first arrivals. Third, different from that of the crustal P wave, the ray path of the head wave,  $P_n$ , always heads downward from the source to the Moho discontinuity to provide additional depth controls over the hypocenter.

### 4.3. Model parameterization and 1D velocity model

In the parameterization of our 1D velocity model, the crust is initially divided into vertical grids of 10 km interval with a constant P wave velocity of 5.8 km/s from 0 to 60 km. The initial Moho depth and  $P_n$  velocity are set as 35 km and 8.1 km/s. These values are estimated from the slope of the travel time curves of the raw data (Fig. 4) and the Crust 2.0 model (Bassin et al., 2000). When employing the 1D joint-inversion scheme (Xu and Song, 2010), a reference 1D velocity model with updated crustal velocities,  $P_n$  velocity, and Moho depth converges after 7 iterations. Finally, our model has a Moho depth of 33.2 km,  $P_n$  velocity of 8.11 km/s, and crustal velocities ranging from 5.72 to 5.91 km/s (Fig. 6).

The 3D crustal velocity model is parameterized into 10 km-spacing vertical grids as 1D model settings and  $0.25^\circ \times 0.25^\circ$  horizontal grids. Grid-spacing of the  $P_n$  velocity model is set as  $0.25^\circ \times 0.25^\circ$  as well. The initial values at grid nodes are given in the final results of 1D velocity model, and the values between nodes (within a grid) are linearly interpolated. The 1D model and earthquake relocation are done jointly together in an iterative process (Fig. 5). Using the final relocated events, after 1D and 3D inversion, the residual distributions are sequentially improved with a convergence of standard deviations from 0.843, 0.415, to 0.371 s (Fig. 7). The root mean square (RMS) of the total travel time residuals drops from 0.857 to 0.371 s or a variance reduction of 81%.

## 5. Model resolution assessment

### 5.1. Ray coverage

After 3 iterations of step 2 (Fig. 5, back and forth between 1D joint inversion and earthquake relocation), 475 earthquakes are relocated

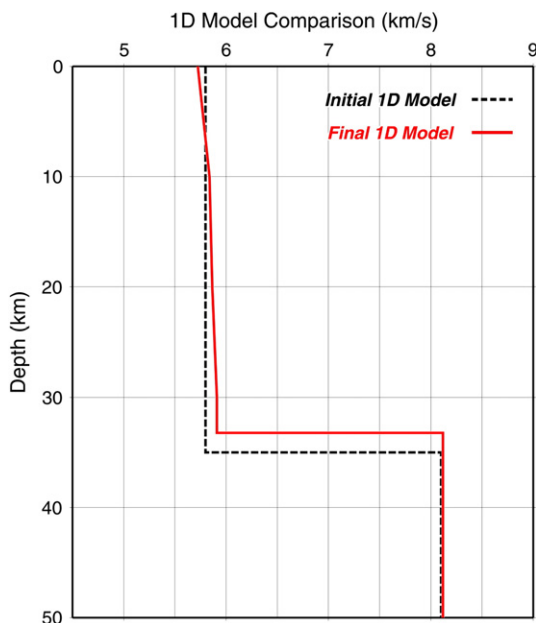


Fig. 6. Initial and final 1D velocity models, which are denoted by the dashed black line and the solid red line respectively.

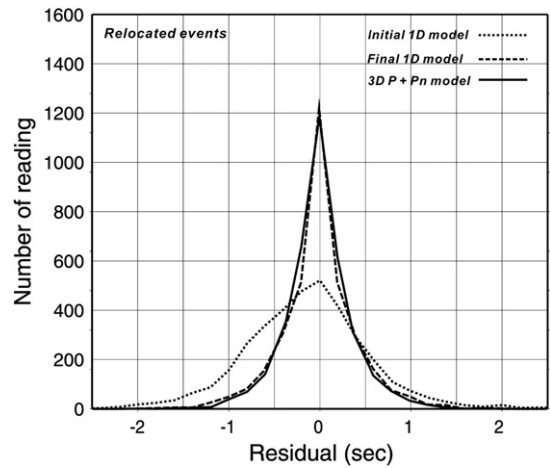


Fig. 7. Residual distribution of the relocated data relative to initial 1D model, final 1D model, and 3D model (combined both crustal P and  $P_n$  models). Derived standard deviations are 0.843, 0.415, and 0.371 sequentially.

and selected (Fig. 8), containing 2425 arrivals of crustal P waves and 1064 arrivals of  $P_n$  waves for the tomographic inversions. It retains about 54% of the raw data. Fig. 9c shows their ray coverage. It fairly covers the model grids in the RRSZ and most of northern Vietnam of our interest.

### 5.2. Resolution tests and performance

We perform a checkerboard test (Leveque et al., 1993) to evaluate the resolution of our tomographic images. In the test, the input model is made as a sinusoidal checkerboard pattern maximum  $\pm 5\%$  velocity perturbation over the 1D model on crustal P and  $P_n$  velocities (Fig. 9a). Several input models with different half-wavelength are tested. Results show that to the half-wavelength of  $0.75^\circ$  we can recovered the checkerboard pattern well in most of the northern Vietnam, in particular at depths of 10 and 20 km in crust, as well as the Moho (Fig. 9b).

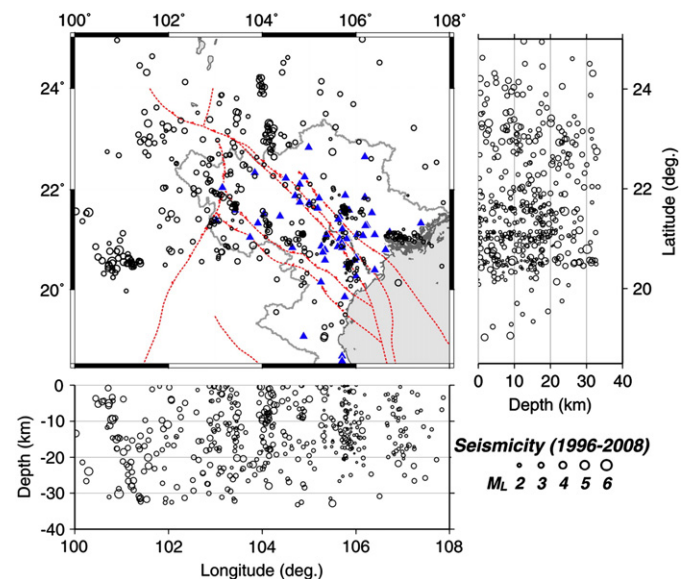
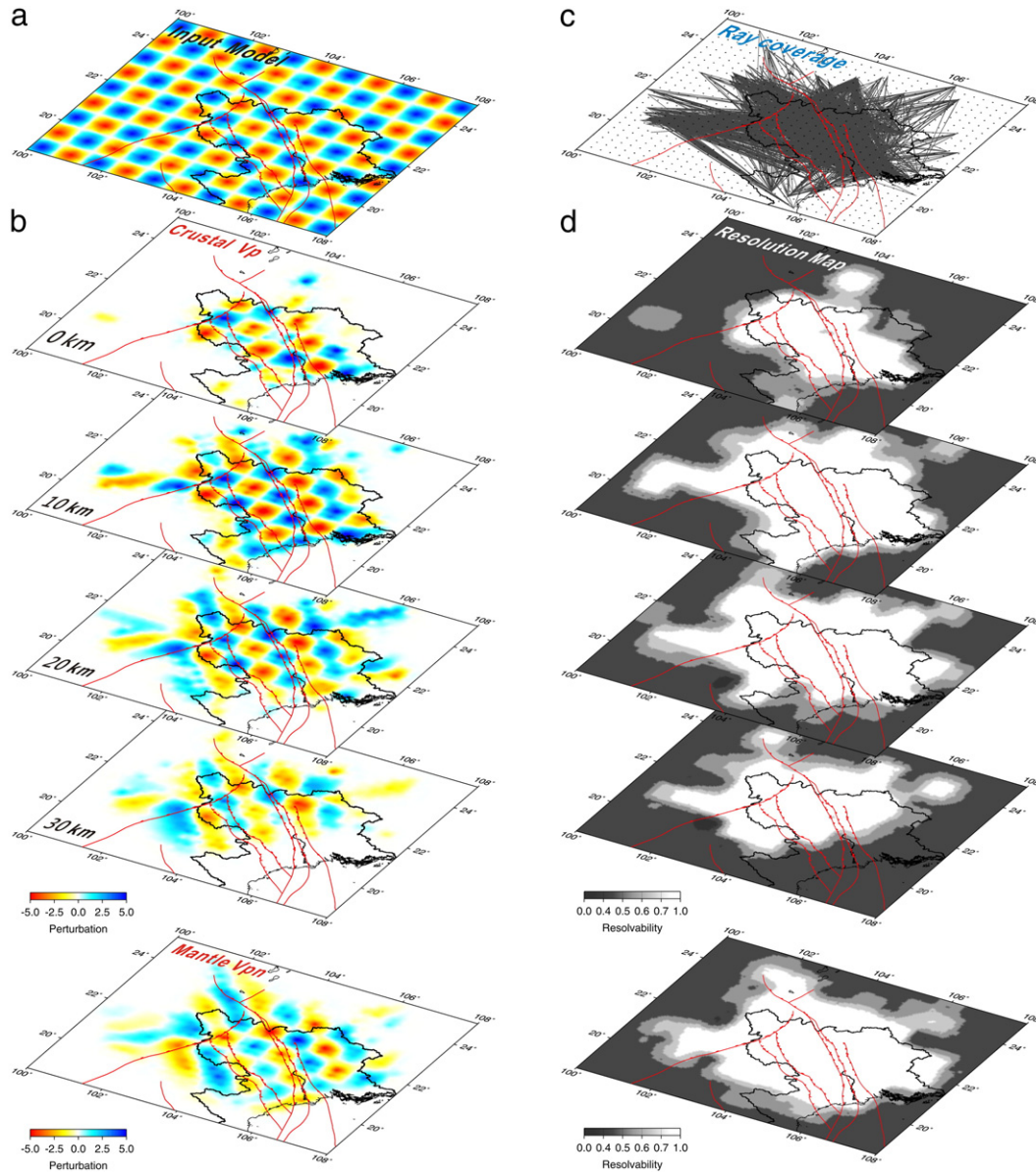


Fig. 8. Distribution map of relocated earthquakes. The red dotted line and blue triangle represent the fault trace and seismic station. Earthquakes are denoted by black circle and scaled by magnitude as legend shows.



**Fig. 9.** Model resolution performance. (a) Input model of checkerboard test with 5% velocity perturbation; (b) resolved results of checkerboard test at 0, 10, 20, 30 km depths for crustal P, and at top of mantle for P<sub>n</sub>; (c) map showing the total crustal P and P<sub>n</sub> ray coverage and our model grid setting; (d) resolution maps derived from checkerboard-test results (Zelt, 1998) at each corresponding depth.

Then, we translate these patterns into the resolution maps quantitatively using the resolvability proposed by Zelt (1998) (see also Liang et al., 2004). The resolvability,  $R$ , from a checkerboard test is defined as:

$$R = \frac{\sum_{i=1}^M (t_i + r_i)^2}{2 \sum_{i=1}^M (t_i^2 + r_i^2)}, \quad (5)$$

where  $t_i$  and  $r_i$  are the true and recovered velocity anomalies at grid  $i$  inside a given area of  $M$  grids. We choose an operating area of  $0.75^\circ \times 0.75^\circ$  centered on the grid for which we want to calculate the resolvability. In our case of  $0.25^\circ$  grid spacing, then  $M$  is equal to 9. A value of resolvability above 0.7 can be viewed as an indication of a well-recovered checkerboard structure (Zelt, 1998). Fig. 9d shows the translated resolution maps, which lend us a criterion to blank out the unreliable areas in tomographic images.

## 6. Results and discussion

Fig. 10a and b displays the results of the 3D crustal P velocity perturbations and the P<sub>n</sub> velocity perturbation map, relative to the 1D reference model (Fig. 6). The station delay times derived from P<sub>n</sub> inversion and their converted Moho depths at each station are shown in Fig. 10c, which shows a range of converted Moho depth around 31–35 km in color.

### 6.1. Correlations with surface geology

At the surface (depth of 0 km), the primary patterns reveal a high velocity belt along the right side of RRSZ and three prominent low velocity spots. We superimpose the rock-type distribution (Fig. 1), and simply regroup it into two main categories: metamorphic/intrusive domain (blue polygons) and volcanic domain (brown polygons). Based on laboratory measurements, metamorphic rocks at shallow depth ca. 20 km have similar wave speeds to intrusive rocks (e.g. granite, granodiorite) but have higher speeds than volcanic rocks (e.g. basalt,

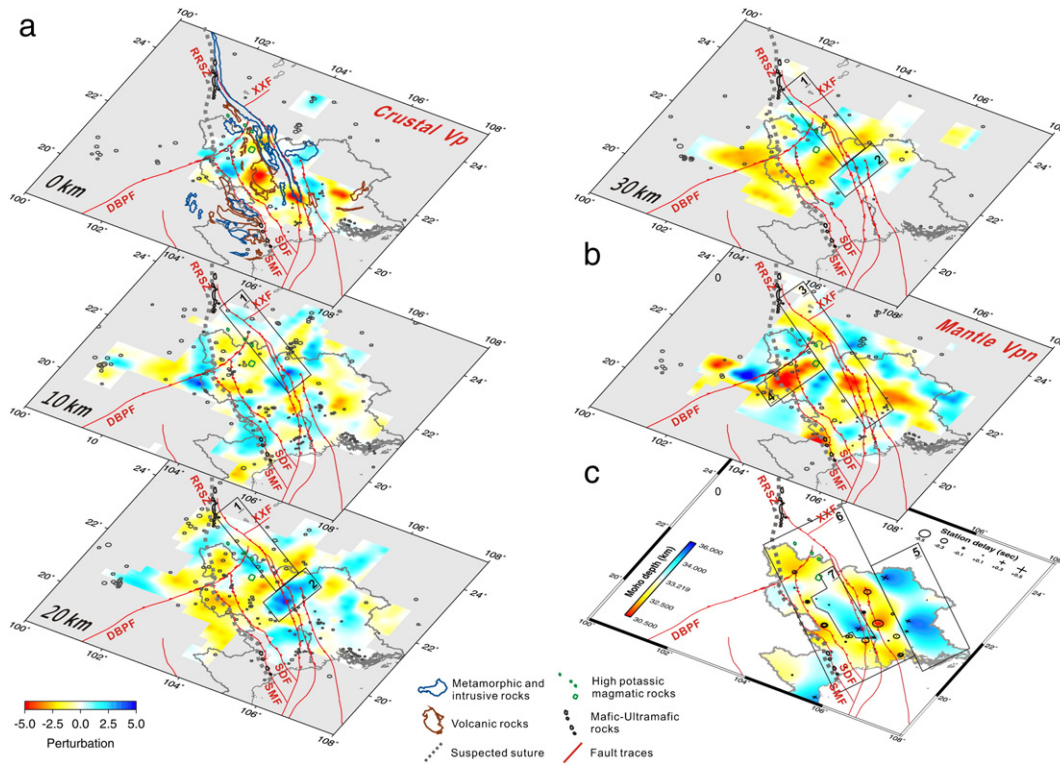


**Fig. 10.** Inversion results for crustal P (a) and mantle-lid  $P_n$  velocities (b), and the derived Moho variation map (c). (a, b) Gray area is blanked by the resolution map (Fig. 9d). The red line and black circle denote the fault traces and the earthquakes projected within 5 km distance above and below. (c) Label shows the station delay times from  $P_n$  velocity inversion. According to the formula (4) (details in text), we translate the delay time into the variation of Moho depth in kilometer, which is shown by color. On the maps, different rock types, suspected suture, and faults are denoted by legend below.

andesite) (Christensen and Mooney, 1995). We observe that the metamorphic/intrusive domains generally correspond to high velocity zones and the volcanic domains to low velocity zones. As do the SCMD to the high velocity anomalies and the loci of high potassic Paleogene magmas to low velocity anomalies. One of the prominent low velocity areas located at the southern tip of the DNCV metamorphic complex does not correspond to a volcanic domain, probably reflecting the site effect of the station in the sediment basin.

6.2. Velocity structures of crust

Down to a depth of 10 km, an apparent high velocity belt still exists (Fig. 10a, box 1) and probably extends to the Tonkin Gulf. This feature disappears in the mid-lower crust (20 and 30 km depth) and becomes a low velocity belt, which is well consistent with the models of Xu et al. (2005) and Lei et al. (2009) in Yunnan province. But a slight difference is that in the mid-lower crust, we observed a NNE–SSW trending high velocity zone (box 2) in the southeastern end of the NW–SE trending low velocity belt (box 1). If considering this NNE–SSW trending pattern encloses the locus where the SCMD is exposed on the surface and does not follow the trend of shear zone, this high velocity zone is likely representative of a metamorphic batholith that results from other tectonic episodes, not coeval with the RRSZ shearing. Many studies have reported that the thermo-tectonic history of the DNCV is more complicated than the Diancangshan and Ailaoshan in Yunnan, and gave much older ages in the Triassic during the Indosinian orogeny (Carter et al., 2001; Searle, 2006). It is suggested that an oblique collision could have occurred between the South China and Indochina blocks with a northwestward migration prior to the developing of India–Eurasia collision and the RRSZ shearing (Carter et al., 2001; Harrison et al., 1992, 1996; Wang et al., 1998, 2000). Our observations reveal a pre-existing metamorphic batholith in the mid-lower crust.

Then, during the RRSZ shearing, this batholith was exhumed and cooled, explaining a more complex thermo-tectonic history of the DNCV metamorphic complex (Searle, 2006; Yeh et al., 2008).

In the meantime, the low velocity belt northwest of the batholith indicates that the material along the shear zone either has relatively high temperature or contains fluid, most likely the water, or maybe both. If the RRSZ is the plate suture where the paleo-Tethys ocean had been consumed, it stands to reason that the water was trapped within the suture and probably became a key to lubricating and facilitating this extremely long structure. As a result, the high velocity belt observed in the upper crust mainly reflects the metamorphism of the RRSZ shearing, but in northern Vietnam, it turns out to be a consequence involving different tectonic phases.

Furthermore, in our model, the mafic/ultramafic ophiolites along the SMF can also be marked well by a high velocity belt (following the dotted line of the suspected suture) at the layer of 10 km depth, but then vanishes at deeper depths. The SMF and SDF were the northward subducting front of the Indochina block and the back-arc opening center in the past (Lepvrier et al., 2004). Followed by a long tectonic evolution of SE Asia, including the India–Eurasia collision afterward, this subduction–arc system turned into an orogenic belt of continent–continent collision and thrust the oceanic crust (i.e. mafic/ultramafic ophiolites) up to the surface. The high velocity belt we detected only at shallower depths probably suggests that the outcrops of mafic/ultramafic ophiolites are restricted in the upper crust as remnant fragments of paleo-oceanic crust.

6.3.  $P_n$  velocities

The NW–SE trending belt with relatively low velocity also appears at the top of the mantle (Fig. 10b, box 3). The velocity of the  $P_n$  wave is rather sensitive to the temperature change in the uppermost

mantle (Black and Braile, 1982), and it therefore is often referred to in the activities of mantle dynamics (Hearn, 1984, 1996; Liang et al., 2004). From this point of view, the low velocity belt may reflect the causal thermal anomalies of the ascending asthenosphere. This implies the heating of the shear zone in the mid-lower crust involves the thermal source from the mantle (Leloup et al., 1999), likely happening during the transtension stage ca. 15.5–30 Ma (Rangin et al., 1995; Searle, 2006). From this point of view, the RRSZ would be a lithospheric structure.

The other conspicuous feature is that the NE–SW striking DBPF seems to be a boundary between the high velocity anomalies to the northwest and the low velocity anomalies to the southeast. This implies that the DBPF is a lithospheric suture of which the depth reaches the top of the mantle and separates two different terrains. However, few studies have discussed the depth dimension of the DBPF. Recently Zhuchiewicz et al. (2004) proposed a conjugate fault system for the RRSZ and DBPF. According to which, if the RRSZ is a lithospheric structure, then the DBPF would be a lithospheric structure to accommodate the relative motions between terrains. But nonetheless, this velocity contrast is located on the fringes of our resolution area. More analysis is required to verify in the future.

#### 6.4. Moho depth variation

In general, the average Moho depth of northern Vietnam we obtained in this study (~33.2 km/s) is similar to results from previous studies in northern Vietnam from receiver functions (~31.4 km, Bai et al., 2010) and in southeast China from deep seismic sounding (32–33 km, Li and Mooney, 1998; Li et al., 2006). Our regional map of Moho depth variation (from our station delays and crustal model) shows several interesting features: First, the Moho depth becomes shallower from northeast to southwest, revealing a thicker crust of South China Block (Fig. 10c, box 5) as previous studies suggest (Bassin et al., 2000; Wu et al., 2004). Second, the crust of northern Vietnam seems to be a local minimum relatively thinner than both sides to the northeast and southwest, implying a consequence of the long and complex thermotectonic history of northern Vietnam (box 6). The loci of high potassic magmatic rocks which are believed to relate to the mantle source, also agrees well with the local thinner crust. Third and most importantly, a prominent depth change of the Moho exhibits just across the RRSZ (box 7). Similar results are also found in Yunnan province, China (Xu et al., 2006), showing an offset of Moho depth on different sides of RRSZ. This is probably the most intuitive evidence to prove the RRSZ is a lithospheric structure that cuts at least the entire crust.

#### 6.5. Continental rheology

The data recorded by the two seismic networks so far are still insufficient to conduct a more detailed tomographic inversion with finer grid-spacing, especially in depths where we only have four nodes (grids) for the crust. However, from the 1D velocity model (Fig. 6), the small increase of velocity with depth in the crust (from 5.72 to 5.91 km/s) is notable. The velocities in mid-lower crust is abnormally low (~5.9 km/s) relative to a regional average of southeast China (~6.3–6.7 km/s, Li et al., 2006), indicating a pure felsic crust without mafic lower crust. A recent study of teleseismic receiver functions show a low Poisson's ratio of crust in northern Vietnam ( $\sigma = 0.23$ , Bai et al., 2010), suggesting the crustal composition composed mainly of metasedimentary and silicic intrusive rocks without mafic or ultramafic components (Christensen, 1996). These types of rocks, with the P wave velocity around 5.5–6.2 km/s (Christensen and Mooney, 1995), are consistent with our results.

We also tried different initial models to test the stability of 1D joint inversion, including the deep sounding model of southeast China (Li and Mooney, 1998; Li et al., 2006). The initial models range from 5.5 to 6.3 km/s in the crust, 28.0 to 40.0 km in the Moho depth,

and 7.5 to 8.5 km/s in the Pn velocity. We obtained very similar 1D models from the different initial models: the crustal velocity changes less than 0.02 km/s, the Moho depth is within about ~1.5 km, and the Pn velocity is within ~0.1 km/s. Thus, the lower crust velocities are very stable and insensitive to the initial models, indicating this feature should be robust. One possible explanation is the intraplate extension, induced by the delamination of thickened continental lithosphere as a response to the India–Asia collision (Chung et al., 1997, 2005). This could have occurred in this region or could result from transported crust by the RRSZ from the Yunnan province of China. The 1D velocity structure, then, represents the portion of the upper-mid crust as the lower crust lost. A recent P wave global tomography, which shows a prominent low velocity belt along the RRSZ in the upper mantle, may also suggest this thermal episode in this region (Li et al., 2008). However, due to the sparse vertical grids in our model, more data sampling the lower crust is needed to confirm the result in the future.

## 7. Conclusions

With a P wave velocity model of crust-to-uppermost mantle, this study aims to provide an insight on the subsurface structures to explore the tectonics of northern Vietnam and to offer additional constraints on the southeastern half of the RRSZ, where seismic investigation has been very limited. Although there have been many studies contributing abundant information to the RRSZ, this study is the first to tomographically explore the 3D velocity structure of northern Vietnam on a finer, local scale. By integrating the records in a period of 1996–2008 from the PBSN and the VSPSN, our results show a fairly good correlation with the surface geology, major structures (especially the RRSZ), and the mantle dynamics. We modify the basic joint inversion approach by Xu and Song (2010) and utilize multiple P waves (crustal and P<sub>n</sub>) to obtain better constraints on the whole crust, the top of the mantle, and the Moho depth.

Our results detect a segmentation of the RRSZ in the mid-lower crust. In the Yunnan province, we obtained similar results with the previous tomographic studies (Lei et al., 2009; Xu et al., 2005), showing a high velocity belt in the upper crust and a low velocity belt in the mid-lower crust along the RRSZ. However, in northern Vietnam, a NNE–SSW trending high velocity zone detected in the mid-lower crust may represent a pre-existing metamorphic batholith with respect to the Indosinian orogeny in the Triassic (Carter et al., 2001). Therefore the DCNV metamorphic complex became an assemblage of the old exhumed metamorphic cores and the later metamorphism of the RRSZ shearing (Searle, 2006; Yeh et al., 2008), contributing to the complex thermo tectonic history (Carter et al., 2001). This segmentation is probably a compromise to the different characteristics between the Red River metamorphic belt in Yunnan and in northern Vietnam. Moreover, the RRSZ is confirmed as a lithospheric structure that cuts through the crust by the observations showing a sharp change of Moho depth just across the RRSZ, and a low velocity belt along the shear zone at top of the mantle. This low velocity belt implies that the RRSZ thermal anomalies in the mid-lower crust are not only a result of the fault shearing but also involve the mantle thermal activities.

Several major structures could also be identified in our model: for instance, the deep root of DBPF, the upper crust remnant of mafic/ultramafic ophiolites, the thickening crust at the margin of the South China block, as well as the low velocity anomalies and locally thin crust beneath the loci of the high potassic Paleogene magmas and P–Tr flood basalts. The last one supports a possibility of intraplate extension extensively occurring in SE Asia at 30–40 Ma (Chung et al., 1997, 2005). Generally, northern Vietnam appears to have a weak crust with a relatively slow and simple 1D velocity structure (Fig. 6) overlying a regionally hot uppermost mantle. This is probably why the seismic activity in northern Vietnam is lower than the surrounding areas, especially comparing with the Yunnan province to the northwest.

## Acknowledgment

This study was supported by the Central Weather Bureau, Taiwan, the National Science Council, Taiwan and the U.S. NSF 0838188. We greatly appreciate the comments and suggestions of Shu-Huei Hung, Yuan-Cheng Cung, Chien-Hsin Chang, Ling-Ho Chung, Yu Wang, Doug Torbeck, and anonymous reviewers of the manuscript that significantly improved it. Special thanks to the Institute of Earth Science, Academia Sinica and Vietnam Earthquake Center for kindly providing the seismic data.

## References

- Allen, C.R., Gillespie, A.R., Han, Y., Sieh, K.E., Zhang, B., Zhu, C., 1984. Red River and associated faults, Yunnan Province, China: Quaternary geology slip rates and seismic hazard. *Geological Society of America Bulletin* 95, 686–700.
- Bai, L., Tian, X., Ritsema, J., 2010. Crustal structure beneath the Indochina Peninsula from teleseismic receiver functions. *Geophysical Research Letters* 37, L24308. doi:10.1029/2010GL044874.
- Bassin, C., Laske, G., Masters, G., 2000. The current limits of resolution for surface wave tomography in North America. *EOS Transactions of the American Geophysical Union* 81, F897.
- Black, P.R., Braile, L.W., 1982.  $P_n$  velocity and cooling of the continental lithosphere. *Journal of Geophysical Research* 87 (B13), 10557–10568.
- Carter, A., Roques, D., Bristow, C., Kinny, P., 2001. Understanding Mesozoic accretion in Southeast Asia: significance of Triassic thermotectonism (Indosinian orogeny) in Vietnam. *Geology* 29, 211–214.
- Christensen, N.I., 1996. Poisson's ratio and crustal seismology. *Journal of Geophysical Research* 101 (B2), 3139–3156.
- Christensen, N.I., Mooney, W.D., 1995. Seismic velocity structure and composition of the continental crust: a global view. *Journal of Geophysical Research* 100 (B7), 9761–9788.
- Chung, S.L., et al., 1997. Intraplate extension prior to continental extrusion along the Ailao Shan–Red River shear zone. *Geology* 25, 311–314.
- Chung, S.L., et al., 2005. Tibetan tectonic evolution inferred from spatial and temporal variations in post-collisional magmatism. *Earth-Science Reviews* 68, 173–196.
- Cong, D.C., Feigl, L.L., 1999. Geodetic measurement of horizontal strain across the Red River Fault near Thac Ba, Vietnam, 1963–1994. *Journal of Geodesy* 73, 298–310.
- Gubbins, D., 1990. *Seismology and Plate Tectonics*. Cambridge University Press, Cambridge.
- Harrison, T.M., Chen, W., Leloup, P.H., 1992. An early Miocene transition in deformation regime within the Red River Fault Zone, Yunnan, and its significance for Indo-Asian tectonics. *Journal of Geophysical Research* 97, 7159–7182.
- Harrison, T.M., Leloup, P.H., Ryerson, F.J., Tapponnier, P., Lacassin, R., Chen, Wenji, 1996. Diachronous initiation of transtension along the Ailao Shan–Red River shear zone, Yunnan and Vietnam. In: Yin, A., Harrison, T.M. (Eds.), *The Tectonic Evolution of Asia*. Cambridge University Press, Cambridge, pp. 208–225.
- Hearn, T.M., 1984.  $P_n$  travel times in southern California. *Journal of Geophysical Research* 89 (B3), 1843–1855.
- Hearn, T.M., 1996. Anisotropic  $P_n$  tomography in the western United States. *Journal of Geophysical Research* 101 (B4), 8403–8414.
- Huang, J., Zhao, D., Zheng, S., 2002. Lithospheric structure and its relationship to seismic and volcanic activity in southwest China. *Journal of Geophysical Research* 107 (B10), 2255. doi:10.1029/2000JB000137.
- Huang, B.S., Le, T.S., Liu, C.C., Toan, D.V., Huang, W.G., Wu, Y.M., Chen, Y.G., Chang, W.Y., 2009. Portable broadband seismic network in Vietnam for investigating tectonic deformation, the Earth's interior, and early-warning systems for earthquakes and tsunamis. *Journal of Asian Earth Sciences* 36, 110–118.
- Lan, C.Y., et al., 2000. Geochemical and Sr–Nd isotopic characteristics of granitic rocks from northern Vietnam. *Journal of Asian Earth Sciences* 18, 267–280.
- Lan, C.Y., Chung, S.L., Lo, C.H., Lee, T.Y., Wang, P.L., Li, H., Toan, D.V., 2001. First evidence for Archean continental crust in northern Vietnam and its implications for crustal and tectonic evolution in Southeast Asia. *Geology* 29, 219–222.
- Lees, J.M., Crosson, R.S., 1989. Tomographic inversion for three-dimensional velocity structure at Mount St. Helens using earthquake data. *Journal of Geophysical Research* 94, 5716–5728.
- Lei, J., Zhao, D., Su, Y., 2009. Insight into the origin of the Tengchong intraplate volcano and seismotectonics in southwest China from local and teleseismic data. *Journal of Geophysical Research* 114, B05302. doi:10.1029/2008JB005881.
- Leloup, P.H., et al., 1995. The Ailao Shan–Red River shear zone (Yunnan, China), Tertiary transform boundary of Indochina. *Tectonophysics* 251, 3–84.
- Leloup, P.H., Ricard, Y., Battaglia, J., Lacassin, R., 1999. Shear heating in continental strike-slip shear zones: model and field examples. *Geophysical Journal International* 136, 19–40.
- Lepvrier, C., Maluski, H., Tich, V.V., Leyreloup, A., Thi, P.T., Vuong, N.V., 2004. The Early Triassic Indosinian orogeny in Vietnam (Truong Son Belt and Kontum Massif): implications for the geodynamic evolution of Indochina. *Tectonophysics* 393, 87–118.
- Leveque, J.J., Rivera, L., Wittlinger, G., 1993. On the use of the checker-board test to assess the resolution of tomographic inversions. *Geophysical Journal International* 115, 313–318.
- Li, S., Mooney, W.D., 1998. Crustal structure of China from deep seismic sounding profiles. *Tectonophysics* 288, 105–113.
- Li, S., Mooney, W.D., Fan, J., 2006. Crustal structure of mainland China from deep seismic sounding data. *Tectonophysics* 420, 239–252.
- Li, C., van der Hilst, R.D., Engdahl, E.R., Burdick, S., 2008. A new global model for P wave speed variations in Earth's mantle. *Geochemistry, Geophysics, Geosystems* 9, Q05018. doi:10.1029/2007GC001806.
- Liang, C.T., Song, X.D., Huang, J.L., 2004. Tomographic inversion of  $P_n$  travel times in China. *Journal of Geophysical Research* 109, B11304. doi:10.1029/2003JB002789.
- Paige, C.C., Saunders, M.A., 1982a. Algorithm 583 – LSQR: sparse linear equations and least squares problems. *ACM Transactions on Mathematical Software* 8 (2), 195–209.
- Paige, C.C., Saunders, M.A., 1982b. LSQR: an algorithm for sparse linear-equations and sparse least-squares. *ACM Transactions on Mathematical Software* 8 (1), 43–71.
- Rangin, C., Klein, M., Roques, D., Le Pichon, X., Trong, L.V., 1995. The Red River Fault system in the Tonkin Gulf, Vietnam. *Tectonophysics* 243, 209–222.
- Searle, M.P., 2006. Role of the Red River shear zone, Yunnan and Vietnam, in the continental extrusion of SE Asia. *Journal of the Geological Society of London* 163, 1025–1036.
- Tapponnier, P., Peltzer, G., Le Dain, A.Y., Armijo, R., Cobbold, P., 1982. Propagating extrusion tectonics in Asia: new insights from simple experiments with plasticine. *Geology* 10, 611–616.
- Tapponnier, P., Peltzer, G., Armijo, R., 1986. On the mechanics of the collision between India and Asia. *Geological Society of London* 19, 113–157.
- Tapponnier, P., et al., 1990. The Ailao Shan/Red River metamorphic belt; Tertiary left lateral shear between Indochina and South China. *Nature* 343, 431–437.
- Trung, N.M., Tsujimori, T., Itaya, T., 2006. Honvong serpentinite body of the Song Ma Fault zone, Northern Vietnam: a remnant of oceanic lithosphere within the Indochina–South China suture. *Gondwana Research* 9, 225–230.
- Van der Hilst, R.D., Engdahl, E.R., 1992. Step-wise relocation of ISC earthquake hypocenters for linearized tomographic imaging of slab structure. *Physics of the Earth and Planetary Interiors* 75, 39–53.
- Wang, P.L., Lo, C.H., Lee, T.Y., Chung, S.L., Lan, C.Y., Yem, N.T., 1998. Thermochronological evidence for the movement of the Ailao Shan–Red River shear zone: a perspective from Vietnam. *Geology* 26, 887–890.
- Wang, P.L., Lo, C.H., Chung, S.L., Lee, T.Y., Lan, C.Y., Thang, T.V., 2000. Onset timing of left-lateral movement along the Ailao Shan–Red River Shear Zone:  $^{40}\text{Ar}/^{39}\text{Ar}$  dating constraint from the Nam Dinh Area, northeastern Vietnam. *Journal of Asian Earth Sciences* 18, 281–292.
- Wang, C.Y., Chan, W.W., Mooney, W.D., 2003. Three-dimensional velocity structure of crust and upper mantle in southwestern China and its tectonic implications. *Journal of Geophysical Research* 108 (B9), 176–193. doi:10.1029/2002JB001973 2442.
- Wu, H.H., Tsai, Y.B., Lee, T.Y., Lo, C.H., Hsieh, C.H., Toan, D.V., 2004. 3-D shear wave velocity structure of the crust and upper mantle in South China Sea and its surrounding regions by surface wave dispersion analysis. *Marine Geophysical Research* 25, 5–27. doi:10.1007/s11001-005-0730-9.
- Xu, Z.J., Song, X., 2010. Joint inversion for crustal and  $P_n$  velocities and Moho depth in Eastern Margin of the Tibetan Plateau. *Tectonophysics* 491, 185–193.
- Xu, Y., Liu, J., Liu, F., Song, H., Hao, T., Jiang, W., 2005. Crust and upper mantle structure of the Ailao Shan–Red River Fault Zone and adjacent regions. *Science in China, Series D: Earth Sciences* 48 (2), 156–164.
- Xu, M., Wang, L., Liu, J., Zhong, K., Li, H., Hu, D., Xu, Z., 2006. Crust and uppermost mantle structure of the Ailaoshan–Red River Fault from receiver function analysis. *Science in China, Series D: Earth Sciences* 49 (10), 1043–1053.
- Yeh, M.W., Lee, T.Y., Lo, C.H., Chung, S.L., Lan, C.Y., Anh, T.T., 2008. Structural evolution of the Day Nui Con Voi metamorphic complex: implications on the development of the Red River Shear Zone, Northern Vietnam. *Journal of Structural Geology* 30, 1540–1553.
- Zelt, C.A., 1998. Lateral velocity resolution from three-dimensional seismic refraction data. *Geophysical Journal International* 135, 1101–1112.
- Zhang, L.S., Scharer, U., 1999. Age and origin of magmatism along the Cenozoic Red River shear belt, China. *Contributions to Mineralogy and Petrology* 134, 67–85.
- Zhang, H., Thurber, C., 2006. Development and applications of double-difference seismic tomography. *Pure and Applied Geophysics* 163, 373–403.
- Zhu, M., Graham, S., McHargue, T., 2009. The Red River Fault Zone in the Yinggehai Basin, South China Sea. *Tectonophysics* 476, 397–417.
- Zhuchiewicz, W., Cuong, N.Q., Bluszcz, A., Michalik, M., 2004. Quaternary sediments in the Dien Bien Phu Fault Zone, NW Vietnam: a record of young tectonic processes in the light of OSL-SAR dating results. *Geomorphology* 60, 269–302.